https://doi.org/10.5194/egusphere-2025-3084
Preprint. Discussion started: 1 September 2025

Evolution of water-soluble organic carbon in neglected coal dust particles influenced by ozone aging

Yuanyuan Qin[1,2,5], Lin Yi[2], Peng Yi[1,3], Juanjuan Qin[2], Xueming Zhou[2], Chenglong Zhang[4], Zhao Shu[2], Yuwei Gao[2], Jihua Tan[2], Lin Zhao[1],

[1] School of Environmental Science and Engineering, Tianjin University, Tianjin 300072, China
[2] College of Resources and Environment, University of Chinese Academy of Sciences, Beijing 100049, China
[3] State Key Laboratory of Environmental Criteria and Risk Assessment, Chinese Research Academy of Environmental Sciences, Beijing 100012, China
[4] Research Center for Eco-Environmental Sciences, Chinese Academy of Sciences, Beijing 100085, China
[5] Guangzhou Institute of Geochemistry, Chinese Academy of Sciences, Guangzhou 510640, China

Correspondence to: Peng Yi (yipeng@craes.org.cn) and Jihua Tan (tanjh@ucas.ac.cn)

https://doi.org/10.5194/egusphere-2025-3084
Preprint. Discussion started: 1 September 2025

Abstract. Coal mining and utilization generate substantial amounts of coal dust, of which the portion in fine particles can travel long distances and further impact climate and air quality through atmospheric aging processes. However, the evolutionary behavior of water-soluble organic carbon (WSOC) in fine coal dust remains unclear. In this study, the aging of coal dust particles and their WSOC processed by ozone (O_3) under dark conditions was investigated in a flow tube reactor. Results show that O_3 aging significantly enhanced the hydrophilicity, light absorption, and fluorescence intensity of WSOC. During the aging process, both carbon loss and gain were observed in WSOC, with the amount of carbon gain exceeding lost through the generation of volatile species. Although the mass absorption efficiency (MAE_{365}) of fresh WSOC was initially low, the O_3 aging process significantly increased the MAE_{365} of WSOC by a factor of 8.8 to 18.2 through the formation of strongly absorbing hydrophilic conjugated compounds. The radiative forcing of WSOC may be underestimated if WSOC absorption linked to atmospheric aging is not accounted for in models. These findings suggest that the long-term O_3 aging effect on coal dust may become prevalent in the background of the complex atmospheric particulate matter and O_3 pollution in China, policymakers should reconsider air quality improvement strategies.

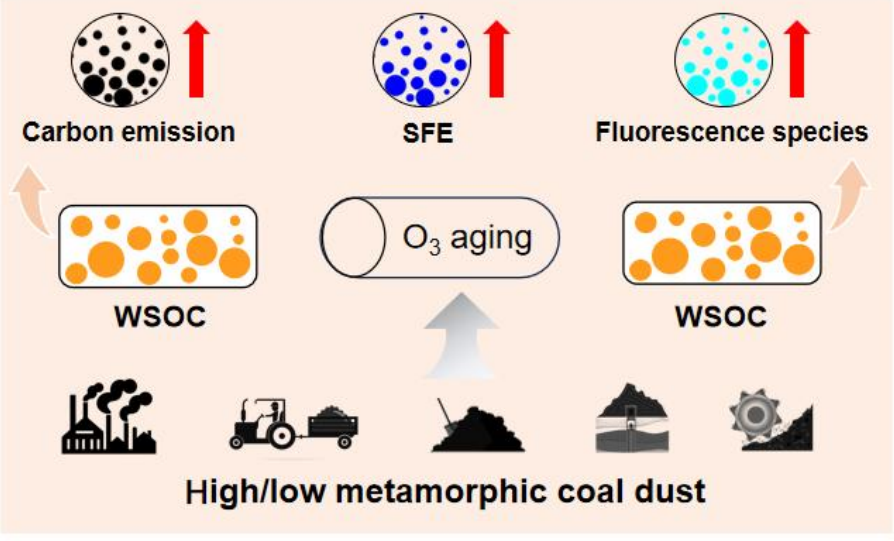

Graphical abstract

https://doi.org/10.5194/egusphere-2025-3084
Preprint. Discussion started: 1 September 2025

1 Introduction

Coal continues to play a crucial role in global energy supply and economic development (Azam et al., 2024). Coal mining and utilization involve complex operations, including underground and open-pit mining, loading, unloading, transportation, and storage (Kasap and Subaşı, 2017). During these processes coal is subject to various mechanical forces, resulting in fragmentation and generation of substantial amounts of coal dust, which is one of the main challenges facing the coal mining industry. Coal dust has long-term impacts on the surrounding environment and public health (Khan et al., 2017). Inhalation of coal dust can induce coal workers pneumoconiosis, with approximately 1,900 people die from the disease in China each year (Zhou et al., 2025).

It is generally believed that coal dust primarily consists of coarse particles. However, recent studies have found that coal dust emitted into the environment is mostly fine particles due to the influence of new mining methods and dust suppression techniques (Abbasi et al., 2021; Zhou et al., 2024). This suggests that the environmental, health, and climatic impacts of coal dust may be underestimated previously since fine particles have longer life-time in air and are generally more toxic than coarse particles (Cardoso, 2015). Furthermore, the mechanization and increasing mining activities have continuously increased emissions of coal dust with finer particle sizes (Abbasi et al., 2021; Zhou et al., 2024). Zhou et al. (Zhou et al., 2024) estimated the coal dust emissions from various mining activities, revealing that $PM_{2.5}$ emissions in China from underground operations, open-pit mining, and train transportation were 31000, 45000, and 18000 tons/year, respectively, with carbonaceous aerosols amounting to 18000, 28000, and 12000 tons/year. According to the emission factors for coal dust stipulated by the China's Ministry of Ecology and Environment, the national total $PM_{2.5}$ emissions from loading and storage processes were estimated at 29600 and 12400 tons/year, respectively, with carbonaceous aerosols at 16000 and 9000 tons/year. The total $PM_{2.5}$ and carbonaceous aerosol emissions from these five processes were 136000 and 84000 tons/year, respectively.

The impact of coal dust on air quality, ecological environment, and human health has been a widespread concern worldwide (Guo, 2021). Earlier studies on coal dust mostly focused on its physicochemical characteristics (e.g., morphology and chemical composition) and impact on human health (Mischler et al., 2016; Vanka et al., 2022; Kamanzi et al., 2023), with very limited knowledge on its aging behavior in the atmospheric environment (Khan et al., 2017; Coppola et al., 2022).

https://doi.org/10.5194/egusphere-2025-3084
Preprint. Discussion started: 1 September 2025

The atmospheric aging processes of coal dust play a crucial role in determining its impact on both the ecological environment and human health, as it can travel for thousands of kilometers in the atmosphere. The chemical composition of coal dust is complex, containing a significant amount of organic and inorganic substances (Xu et al., 2017), among which water-soluble organic compounds (WSOC), as a crucial component of $PM_{2.5}$ (Horník et al., 2021), significantly affect air quality and climate change (Snyder et al., 2009; Sun et al., 2011; Chen et al., 2020). The formation and transformation of WSOC in atmospheric particulate matter are highly complex (Xiang et al., 2017), particularly during aging process, which can significantly alter its physical and chemical properties. Studies on the aging behavior of WSOC in particulate matter emitted from some mainstream sources (e.g., biomass burning and coal combustion), are relatively well-established (Li et al., 2020; Kuang et al., 2021). However, the aging behavior of WSOC in coal dust, an often-overlooked source of fine particulate matter, remains unknown. Given that prolonged atmospheric exposure of coal dust inevitably induces complex WSOC transformations through interactions with atmospheric constituents, this neglected evolutionary process warrants in-depth investigation.

This study aims to systematically investigate the effects of O_3 aging on coal dust and its WSOC. To this end, Fourier-transform infrared spectroscopy (FTIR) and X-ray photoelectron spectroscopy (XPS) were employed to analyze the chemical structural changes of coal dust particles, and high-performance liquid chromatography (HPLC) was used to monitor gaseous pollutants emitted during the aging process to assess the environmental impact of coal dust particles. Furthermore, the aging behavior of WSOC was investigated using a combination of three-dimensional fluorescence spectroscopy, ultraviolet-visible absorbance spectroscopy, and FTIR. Through a systematic study of coal dust particles and their water-extractable organic components, this research provides new insights into the oxidation processes of coal dust in the atmosphere and its environmental behavior, as well as offering a scientific basis for environmental protection during coal mining and utilization processes.

https://doi.org/10.5194/egusphere-2025-3084
Preprint. Discussion started: 1 September 2025

2 Sampling and analytical methods

2.1 Sample collection and preparation

Coal mined in China primarily consists of medium and high metamorphic coal. Coal production in Shanxi province and Inner Mongolia Autonomous Region accounted for over 50% of the national total production (Liu et al., 2023). In this study, three high metamorphic coal dust (HMC-D) samples were collected from the ventilation outlets of a coal mine in Shanxi Province. Additionally, three medium metamorphic coal dust (MMC-D) samples were collected from the ventilation outlets of different mining areas in Inner Mongolia. To adhere to safety measures, brushes were employed to collect these samples from the inner walls of air outlets within the coal mine shafts. To prevent contamination, all samples were promptly stored in securely sealed bags and refrigerated for subsequent laboratory analysis.

2.2 Particle aging experiments

The aging of coal dust particles was conducted using a flow tube reactor, which simulates particle aging under controlled environmental and chemical conditions. Figure 1 shows the schematic diagram of the flow tube reactor, which consists of three main components: the intake system, the reaction system, and the detection system. These components are interconnected by polytetrafluoroethylene (PTFE) tubing. Prior to the experiments, the reactor was continuously cleaned with high-purity N_2 for over 2 h until the O_3 concentration was reduced below the detection limit. O_3 gas was generated by passing high-purity O_2 through an O_3 generator, and the generated O_3 gas was introduced into the flow tube reactor. To simulate the exposure cycle that coal dust may undergo in real atmospheric environments, a relatively high O_3 concentration of 2 ppm was used for the O_3 aging process. All samples of each high/low metamorphic coal dust were mixed together and placed on glass slides and exposed to the reactor environment under following conditions: 2 ppm O_3 concentration, 40% relative humidity (RH), and room temperature (23.0 °C–23.9 °C) for aging durations of 0, 3, 6, 9, and 12 h under dark conditions. This exposure is equivalent to an exposure period of up to 13 days in the real atmosphere, assuming an ambient concentration of 75 ppb (the concentration limit of Ambient Air Quality Standards of China, level 2). Previous study has demonstrated that the oxidation products and oxidation mechanisms of BrC are similar under both relatively high (1–23.6 ppm) and low (45–230 ppb) O_3 concentrations (Kuang and Shang, 2020). Thus, the O_3 aging behavior of WSOC observed in

https://doi.org/10.5194/egusphere-2025-3084
Preprint. Discussion started: 1 September 2025

this study is comparable to the aging behavior in actual atmospheric environments with lower O_3 concentrations.

To eliminate the interference from high O_3 concentrations during the carbonyl compound collection process, a KI-filled pre-column was placed before the DNPH and O_3 concentration in the reactor was at a lower level of 200 ppb. Carbonyls in the outlet of reactor were collected using 2,4-dinitrophenylhydrazine (DNPH) through an autosampler (Jinji Technology (Beijing) Co., Ltd., China) at a flow rate of 1.6 L/min. Each sample was collected continuously for 3 h, with sampling being carried out up to 18 h. Prior to sample collection, blank samples were obtained under the same experimental conditions for background correction.

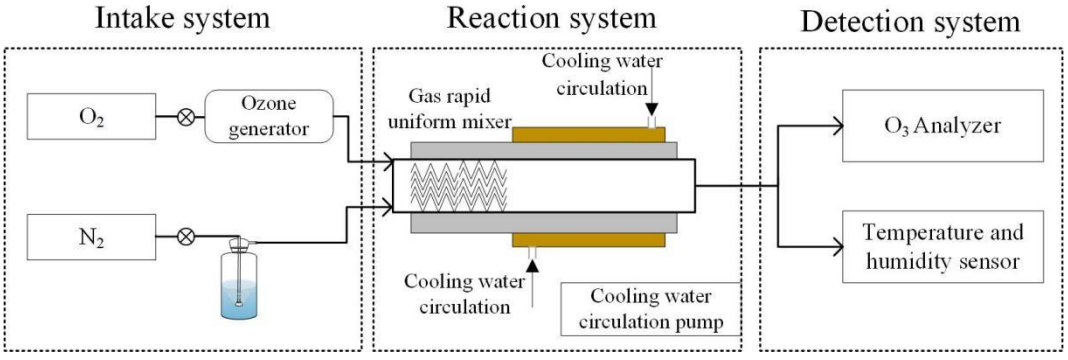

Figure 1. The schematic diagram of the flow tube reactor

2.3 WSOC extraction

1.6 g coal dust sample was extracted with 30 mL Milli-Q water via ultrasonication for 30 min to ensure the extensive release of solubilized WSOC. The extracted liquid was then filtered through a 0.22 μm membrane filter to remove insoluble suspensions. Blank samples, used for background checks, were extracted under the same conditions.

2.4. Chemical analysis

2.4.1 Carbonaceous species and elements analysis

5 mg coal dust was evenly spread on a quartz filter and loaded into the sample chamber of a thermal/optical carbon analyzer (model-4, Sunset Laboratory Inc, USA) to measure organic carbon (OC) and elemental carbon (EC). The temperature protocols followed the IMPROVE Thermal/Optical method, as modified by the Desert Research Institute. WSOC

https://doi.org/10.5194/egusphere-2025-3084
Preprint. Discussion started: 1 September 2025

concentration was determined with a total organic carbon analyzer (Analytic Jena AG multi N/C3100, Germany). Prior to the WSOC determination, samples were acidified with 2 M HCl to eliminate inorganic carbon interference. Organic carbon was converted to CO_2 via catalytic oxidation at 680 °C and quantified with a non-dispersive infrared detector. For elemental analysis, a suite of elements (Li, Na, Mg, Al, K, Ca, V, Mn, Fe, Co, Cu, Zn, As, Se, Rb, Cd, Pb, and Bi) was extracted via microwave digestion with 7 mL of ultrapure water, 2 mL of HNO_3, and 1 mL of H_2O_2. The extracted elements were subsequently analyzed by inductively coupled plasma-mass spectrometry (ICP-MS, iCAP Q, Thermo Scientific, Germany).

2.4.2 UV−Vis absorption spectra and EEM fluorescence spectra

The UV−Vis absorption and three-dimensional excitation-emission matrix (EEM) fluorescence spectra of WSOC were measured using a 1 cm path-length quartz cell. UV-Vis absorption spectra were obtained with a UV-visible spectrophotometer (UV-2401PC, Shimadzu, Japan), covering a wavelength range of 200 to 500 nm with an interval of 1 nm. EEM fluorescence spectra were determined with a fluorescence spectrophotometer (Agilent Cary Eclipse, America), with excitation wavelengths ranging from 200 to 400 nm and emission wavelengths from 250 to 500 nm, both with an interval of 5 nm.

2.4.3 Carbonyls analysis

The analysis of carbonyl compounds was performed in accordance with EPA Method TO-11A (EPA., 1999). Carbonyls were collected on cartridges and subsequently eluted with 5 mL of acetonitrile (LC/MS grade, Fisher Chemical). The eluates were analyzed using a high-performance liquid chromatography (HPLC) (LC3000, Wayeal, Inc., China). Separation was achieved on a 4.6×250 mm Inertsil ODS-P C18 column. The gradient elution started with solvent I (acetonitrile/ultrapure water, 2/1, v/v) for 8 min, followed by a linear increase to solvent II (acetonitrile/ultrapure water, 3/1, v/v) over 4 min, then to 100% acetonitrile over 6 min, which was held for 7 min, and finally returned to solvent I over 2 min, and then hold for 5 min. The flow rate of elution solvent was set at 0.8 mL/min. Prior to each analysis, the detector baseline was checked to ensure stable conditions.

https://doi.org/10.5194/egusphere-2025-3084
Preprint. Discussion started: 1 September 2025

2.4.4 FTIR and XPS Analysis

FTIR Analysis: The functional groups of WSOC and coal dust were analyzed using an ATR-FTIR spectrometer: Vertex 70 (Bruker, Germany) for WSOC and Nicolet iN10MX (Thermo Scientific, USA) for coal dust. For the analysis, a fully dried mixture of lyophilized WSOC and coal dust was placed on the specimen holder. FTIR spectra were recorded over the range of 4000 to 400 cm^{-1} with a spectral resolution of 4 cm^{-1} and a data interval of 1 cm^{-1}.

XPS Analysis: The elemental composition and molecular structure of the coal dust samples were examined using X-ray Photoelectron Spectroscopy (XPS, ESCALAB 250Xi, Thermo Scientific, USA). The types of oxygen-functional groups present in the coal dust were identified through XPS peak deconvolution and associated calculations, both before and after sample modification, along with their relative abundances. The analysis was conducted with a monochromatic Al Kα excitation source (hv=1486.6 eV) and an Energy Step Size of 0.050 eV. The binding energy of C1s at 284.8 eV was used as the reference for energy calibration.

2.5 Data analysis

2.5.1 UV-Vis absorption spectra

The mass absorption efficiency (MAE_λ, m^2/g), derived from UV-Vis absorption spectra, was calculated using the following formula (Jane et al., 2017):

$$MAE_\lambda = \frac{A_\lambda}{C \cdot L} \cdot \ln(10) \quad (1)$$

where A_λ refers to the absorbance at wavelength λ, C is the mass concentration of WSOC (mg/L), and L is the cell path length (1 cm).

2.5.2 EEM analysis

The raw EEM spectra were meticulously processed as detailed in literature (Xiao et al., 2018). Background correction was performed by subtracting the EEM spectra of pure water from the EEM spectra of WSOC. The UV-Vis absorbance in the 200-500 nm wavelength range was used to correct the inner-filter effect on the fluorescence intensity. Following these corrections, the Raman peak area of pure water was used to normalize the fluorescence intensity to Raman units (RU). The

https://doi.org/10.5194/egusphere-2025-3084
Preprint. Discussion started: 1 September 2025

normalized fluorescence intensity was then divided by the TOC concentration to calculate the specific fluorescence intensity per unit TOC. The fluorescence indices were calculated as follows:

$$\frac{\mathrm{AFI}}{\mathrm{TOC}} = \frac{1}{\mathrm{TOC}}\left(\frac{1}{N}\sum_{\mathrm{Ex}}\sum_{\mathrm{Em}} I\right) \quad (2)$$

$$\mathrm{HIX} = \frac{\mathrm{EEM}_{\mathrm{Ex254,\ Em435\text{-}480}}}{\mathrm{EEM}_{\mathrm{Ex254,\ Em300\text{-}345}}} \quad (3)$$

$$\mathrm{Peak\ (T/C)} = \frac{\mathrm{EEM}_{\mathrm{Ex274,\ Em350}}}{\max(\max(\mathrm{EEM}_{\mathrm{Ex320\text{-}340,\ Em410\text{-}430}}))} \quad (4)$$

where FI denotes fluorescence intensity, *I* represents the fluorescence intensity at each Ex/Em wavelength position, and *N* is the total number of EEM data.

2.5.3 Simplified forcing efficiency (SFE)

The potential direct radiative effect of WSOC was estimated using the simple forcing efficiency (SFE, W/g) method described by Chen and Bond (2010) as follows (Chen and Bond, 2010):

$$\mathrm{SFE} = -\frac{1}{4}S(\lambda)\tau_{atm}^2(1\text{-}F_c)\times[2(1-\alpha_s)^2\times\beta\times\mathrm{MSC}(\lambda) - 4\alpha_S\times\mathrm{MAC}(\lambda)] \quad (5)$$

where $S(\lambda)$ denotes the solar irradiance, obtained from the ASTM G173-03 reference spectra, τ_{atm} is the atmospheric transmission (0.79), F_c is the cloud fraction (0.6), a_s is the surface albedo (0.19), β and $\mathrm{MSC}(\lambda)$ represent the backscatter fraction and mass scattering efficiency of the particles, respectively, which was not considered in this study. $\mathrm{MAC}(\lambda)$ is the mass absorption efficiency of carbonaceous aerosols, was evaluated only at 365 nm.

3 Results and discussion

3.1 Chemical composition of coal dust

Analysis of coal dust samples reveals consistent particle size distributions, peaking between 3.5 and 4.0 μm (Zhou et al., 2024). The coal dust generated during mining operations is primarily influenced by factors such as mining technology and equipment, operations and management, geological conditions, and transportation and loading processes. However, the most significant influence arises from the occurrence state of the coal seam. Coal dust primarily consists of organic and inorganic

https://doi.org/10.5194/egusphere-2025-3084
Preprint. Discussion started: 1 September 2025

components. Specifically, Carbon (C) accounts for 80.1% and 70.4% of the total mass of HMC-D and MMC-D, respectively, of which 22.3% and 34.5% were organic carbon (OC) and 57.8% and 35.9% were elemental carbon (EC). The inorganic components include oxides of silicon, aluminum, iron, calcium, magnesium, potassium, and sodium. The content ranges for these elements in the two samples are approximately 7.72% to 9.62% for silicon (Si), 4.91% to 6.24% for aluminum (Al), 1.53% to 1.97% for iron (Fe), and 1.24% to 3.55% for calcium (Ca). The top five trace elements are titanium (Ti), zinc (Zn), strontium (Sr), barium (Ba), and manganese (Mn), with concentrations of 2746.4, 431.6, 296.4, 261.0, and 252.0 μg/g, respectively.

3.2 Variations in coal dust characteristics

3.2.1 FTIR analysis

The chemical structure of coal dust particles was determined using FTIR and X-ray photoelectron spectroscopy (XPS). In the FTIR spectra of the two raw coal dust samples (Figure 2), the absorption peaks at 3620–3692 cm^{-1} correspond to the stretching vibrations of O-H bonds, indicating the presence of hydroxyl functional groups on the surface of the coal dust particles, those at 3231–3328 cm^{-1} are associated with N-H bonds (Dai et al., 2022), and those at 2916–3039 cm^{-1} are related to C-H stretching vibrations (Yan et al., 2020). These results suggest that the coal dust samples contain a substantial amount of nitrogen-containing and aromatic compounds. The peaks at 1594-1602 cm^{-1} may be related to C=C or C-H bonds (Ahmad et al., 2023), and the peaks at 1432-1439 cm^{-1} are associated with C-H bonds. In contrast, the MMC-D sample exhibits an absorption peak at 1257 cm^{-1}, corresponding to the stretching vibrations of C-O (Jiao et al., 2022). This difference may reflect variations in the composition of surface functional groups between the two samples. Both samples display a significant absorption peak at 1009 cm^{-1}, likely related to silicate minerals present in the coal dust (Ahmad et al., 2023).

https://doi.org/10.5194/egusphere-2025-3084
Preprint. Discussion started: 1 September 2025

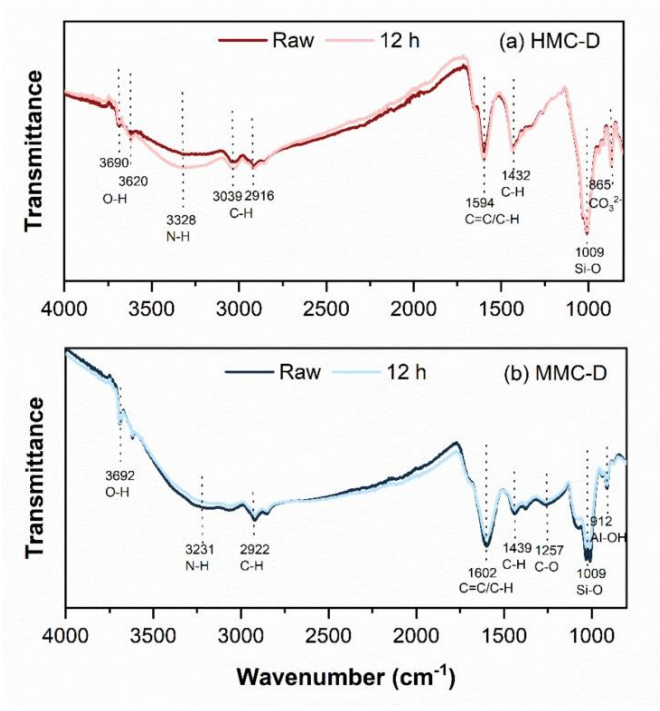

Figure 2. FTIR spectra of raw and aged coal particles in (a) HMC-D and (b) MMC-D.

3.2.2 XPS analysis

To further quantify the changes in the chemical properties of coal dust samples before and after oxidation, XPS analysis was conducted to investigate the types and relative proportions of functional groups. The XPS spectra of two coal dust samples before and after O_3 treatment are shown in Figure 3. XPS detected the presence of functional groups on the surface of coal dust particles, including C-C/C-H (284.8 eV), C-O-C/C-OH (286.0-286.2 eV), and COOH/C=O (289.0 eV) (Zhao et al., 2021; Jiang et al., 2023). The peak areas and percentage of the functional groups, obtained through peak fitting, are shown in Table 1. The C-C/C-H group exhibits the largest peak area, suggesting that its content is the highest among the coal dust samples. After O_3 aging, the proportion of C-C/C-H in the raw HMC-D sample significantly decreases from 94.1% to 90.3%, while the proportions of oxygen-containing functional groups increases. Specifically, the C-O-C/C-OH proportion increases from 5.3% to 7.6%, and the COOH/C=O proportion increases from 0.6% to 2.1%. This phenomenon was not observed in MMC-D sample. These results suggest that the increased surface hydrophilic groups in high-metamorphic coal samples after O_3 aging correspondingly promote more WSOC release. Conversely, in medium-metamorphic coal particles, despite the

https://doi.org/10.5194/egusphere-2025-3084
Preprint. Discussion started: 1 September 2025

decrease in hydrophilic groups, the WSOC content was increased, probably due to other chemical changes in the samples during the aging process (e.g., rearrangement of the surface structure of the particulate matter). In conclusion, FTIR and XPS analyses demonstrate that the chemical structure of coal dust particles undergoes structural changes during oxidation, which also affects the content and characteristics of WSOC.

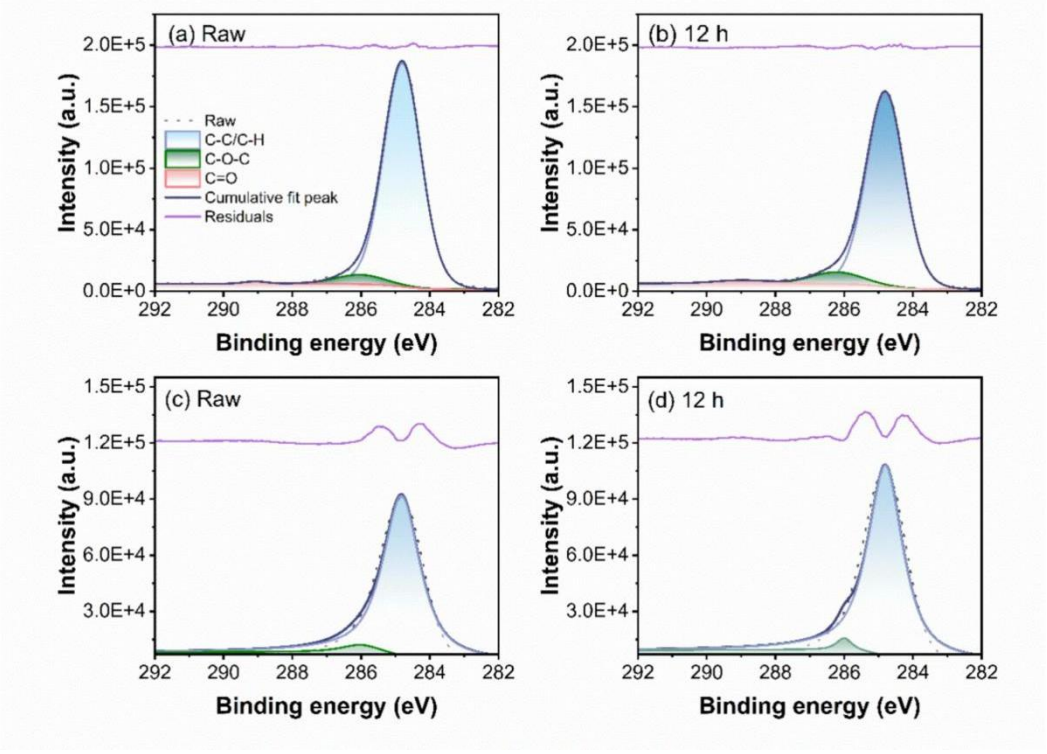

Figure 3. XPS spectra of fresh and aging coal particle in (a, b) HMC-D and (c, d) MMC-D

Table 1. The percentage of the functional groups of fresh and aging coal particles in HMC-D and MMC-D

Peak (eV)	Functional group	FWHM	HMC-D		MMC-D	
			Raw	12 h	Raw	12 h
284.8	C-C/C-H	1.3	94.1%	90.3%	95.1%	97.2%
286.0-286.2	C-O-C/C-OH	1.7	5.3%	7.6%	4.9%	2.8%
289.0	COOH/C=O	0.8	0.6%	2.1%	/	/

https://doi.org/10.5194/egusphere-2025-3084
Preprint. Discussion started: 1 September 2025

3.2.3 Carbonyls analysis

In this study, we further investigate the oxidation products, i.e., carbonyl compounds, generated from coal dust particles during O_3 aging. The identified carbonyl compounds include formaldehyde, acetaldehyde, acetone, crotonaldehyde, butyraldehyde, benzaldehyde, cyclohexanone, isovaleraldehyde, valeraldehyde, m-tolualdehyde, p-tolualdehyde, glutaraldehyde, dimethylbenzaldehyde, heptaldehyde, octanal, glyoxal, and methylglyoxal, as shown in Tables 2 and 3.

The O_3 aging significantly impacts the formation of carbonyl compounds, with varying effects depending on the degree of metamorphism of coal dust samples. Generally, a higher emission of carbonyl compounds was observed during the initial aging phase (3 h). In HMC-D samples, acetone, isovaleraldehyde, and glyoxal were the most abundant, with average concentrations of 0.27, 0.68, and 0.50 μg/m³, respectively. In contrast, the MMC-D samples exhibited higher emissions of formaldehyde, acetaldehyde, and acetone, with average concentrations of 0.82, 0.73, and 8.80 μg/m³, respectively. The O_3 aging may lead to the breakage of C-C bonds in the coal dust samples, resulting in the formation of carbonyl compounds (Fan et al., 2020). Notably, the emission of carbonyl compounds from MMC-D samples was considerably higher than that from HMC-D samples. These carbonyl compounds are important precursors to secondary organic aerosols (SOA) (Ervens, et al., 2007), implying that aging of coal dust could exacerbate the complexity of atmospheric pollution. Given the increasing frequency of O_3 pollution due to accelerated global climate change, it is crucial to remain vigilant about the effects of O_3 aging on particulate matter.

Table 2. Emissions of carbonyl compounds from HMC-D during O_3 aging (μg/m³)

Aging time	3 h	6 h	9 h	12 h	15 h	18 h
Acetaldehyde	1.39	0.24	0.00	0.01	0.00	0.00
Acetone	2.50	0.16	0.00	0.37	0.24	0.83
Crotonaldehyde	0.03	0.63	0.36	0.43	0.72	0.86
Butyraldehyde	0.24	0.19	0.05	0.16	0.07	0.36
Cyclohexanone	0.21	0.22	0.12	0.09	0.10	0.08
Isovaleraldehyde	0.04	1.26	0.01	0.06	1.19	0.95
Valeraldehyde	0.48	0.00	0.09	0.03	0.00	0.00
m-Tolualdehyde	1.12	0.00	0.50	0.00	0.00	0.00
p-Tolualdehyde	0.03	0.00	0.00	0.00	0.00	0.00

https://doi.org/10.5194/egusphere-2025-3084
Preprint. Discussion started: 1 September 2025

Glutaraldehyde	0.06	0.00	0.00	0.00	0.00	0.00
Dimethylbenzaldehyde	0.18	0.18	0.18	0.00	0.14	0.10
Heptaldehyde	0.19	0.00	0.00	0.00	0.00	0.00
Octanal	0.33	0.00	0.05	0.07	0.02	0.00
Glyoxal	0.34	0.57	0.66	0.40	0.96	0.84

Table 3. Emissions of carbonyl compounds from MMC-D during O_3 aging (μg/m^3)

Aging time	3 h	6 h	9 h	12 h	15 h	18 h
Formaldehyde	2.72	1.10	0.67	0.44	0.01	0.00
Acetaldehyde	3.80	0.45	0.14	0.00	0.00	0.00
Acetone	15.4	10.9	8.62	7.54	5.41	4.96
Crotonaldehyde	0.00	0.00	0.24	0.44	0.46	0.81
Butyraldehyde	0.33	0.25	0.25	0.23	0.22	0.22
Benzaldehyde	0.08	0.04	0.03	0.02	0.02	0.00
Cyclohexanone	0.04	0.47	0.28	0.15	0.12	0.07
Isovaleraldehyde	0.35	0.00	0.00	0.00	0.00	0.00
Valeraldehyde	0.00	0.18	0.14	0.09	0.11	0.08
m-Tolualdehyde	0.01	0.00	0.00	0.00	0.00	0.00
p-Tolualdehyde	0.00	0.11	0.09	0.09	0.12	0.06
Glutaraldehyde	0.11	0.03	0.00	0.00	0.00	0.00
Octanal	0.23	0.20	0.08	0.03	0.07	0.00
Glyoxal	0.00	0.00	0.21	0.29	0.33	0.65
Methylglyoxal	0.11	0.06	0.15	0.010	0.02	0.00

3.3 Variations in WSOC characteristics

3.3.1 WSOC content

The variations of WSOC content in coal dust with O_3 aging are shown in Figure 4. For both types of O_3-aged coal dust particles, WSOC content increased sharply from 0 to 6 h, followed by fluctuating changes from 6 to 12 h. Overall, WSOC content increased with increasing O_3 aging time at rates of 0.285 mg/L/h and 0.107 mg/L/h, respectively, for HMC-D and MMC-D. This phenomenon is consistent with previous studies (Decesari et al., 2002). O_3 oxidation of particles can generate

https://doi.org/10.5194/egusphere-2025-3084
Preprint. Discussion started: 1 September 2025

new WSOC fractions (Decesari et al., 2002; Li et al., 2015) and may also break the C=C bonds in weakly or nonpolar organic compounds, resulting in the formation of highly hydrophilic oxygen-containing functional groups on the coal dust surface, thereby enhancing its solubility (Baduel et al., 2011). Furthermore, as discussed in Section 3.2.3, O_3 aging may also lead to the breakage of the C-C bond, producing volatile species and causing carbon loss. However, despite the carbon loss from coal dust particles, the increase in WSOC content suggests that the amount of WSOC components generated during O_3 aging outweighs the carbon lost through the production of volatile species.

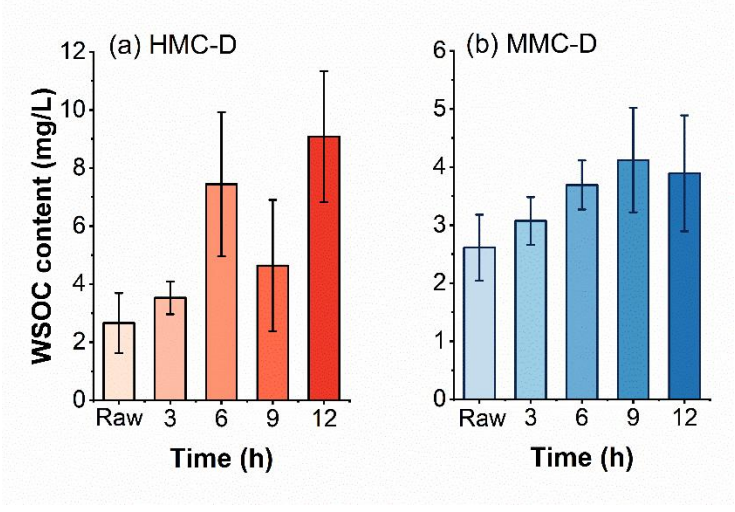

Figure 4. The variations in WSOC content of particles during O_3 aging.

3.3.2 UV-vis spectra

In this study, MAE_{365} was investigated to characterize the evolution of the light-absorbing properties of WSOC during O_3 aging. As shown in Figure 5, the MAE_{365} of WSOC exhibites a general increasing trend, peaking at 12 h, though a decline is observed at 9 h. After 12 h of aging, the MAE_{365} values for WSOC in HMC-D and MMC-D increase by a factor of 8.8 and 18.2, respectively, compared to fresh samples. This suggests that the O_3 aging process dramatically increases the absorption efficiency of WSOC, particularly in lower metamorphic coal samples. The increase in WSOC absorption efficiency can be attributed to two main factors: First, the increase in absorption efficiency may be attributed to the elevated WSOC content (Figure 4), such as aging process leading to the formation of strongly absorbing and hydrophilic conjugate compounds

https://doi.org/10.5194/egusphere-2025-3084
Preprint. Discussion started: 1 September 2025

(Kuang et al., 2021). Second, the structural changes in WSOC during aging, such as the oxidation of aliphatic structures in coals that facilitate oxidative transformations (Table 1). Previous studies have demonstrated that the absorption of BrC in secondary organic aerosol (SOA) increases during O_3 aging due to the formation of carbonyl groups (Sareen et al., 2013). Despite the relatively low light absorption capacity of fresh coal dust, there is a marked enhancement in its light absorption capacity during the aging process. These findings suggest a need to reevaluate the potential impact of WSOC from coal dust sources on atmospheric radiative forcing.

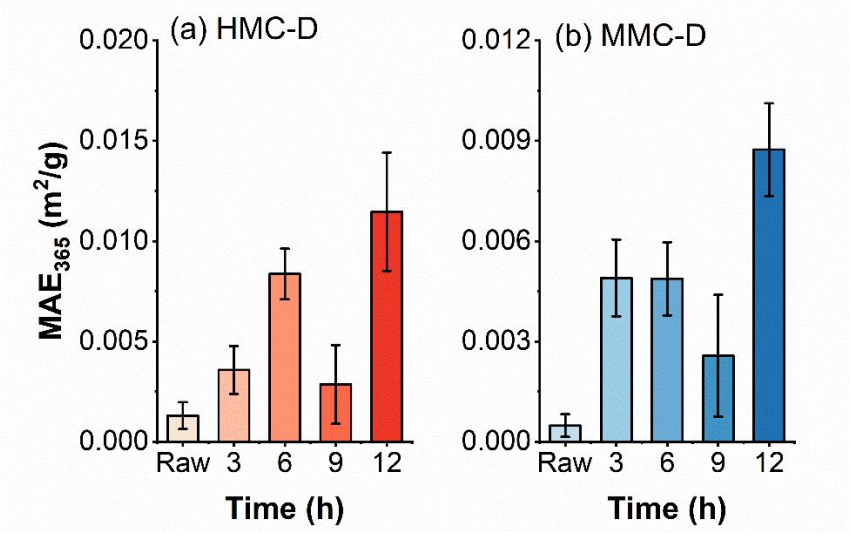

Figure 5. The variations in MAE_{365} of particle extracts during O_3 aging

3.3.3 EEM fluorescence characteristics

As shown in Figure 6, the AFI/TOC of WSOC increases during the O_3 aging process, especially after aging for 12h. The enhancement of fluorescence may be related to the increase in oxygen-containing functional groups in the particles, as shown in Table 1. Chen et al. (Chen et al., 2016a) demonstrated a strong correlation between fluorescent components and chemical groups, such as oxygen-containing functional groups (nonacidic carbonyl C=O and carboxylic COOH groups). Notably, the percentages of the FRI1 and FRI2 components of WSOC in both HMC-D and MMD-D samples gradually decrease with O_3 aging (see Figure 7), while those of FRI3 and FRI5 components significantly increase, with an enhancement factor ranging from 1.30 to 9.34. This indicates that the contribution of aromatic protein-like substances to

https://doi.org/10.5194/egusphere-2025-3084
Preprint. Discussion started: 1 September 2025

WSOC decreases during the aging process, and those of fulvic acids and humic like substances increase significantly (Yang et al., 2020). This change may be linked to the fact that the O_3 oxidation process leads to the decomposition of low molecular weight compounds and the formation of high molecular weight aromatic compounds that are structurally more stable and typically exhibit enhanced fluorescence. The presence of such high molecular weight and highly aromatic compounds usually implies greater environmental persistence. This may indicate that aged WSOC could have a longer residence time in the environment, potentially leading to long-term impacts on both environmental quality and human health.

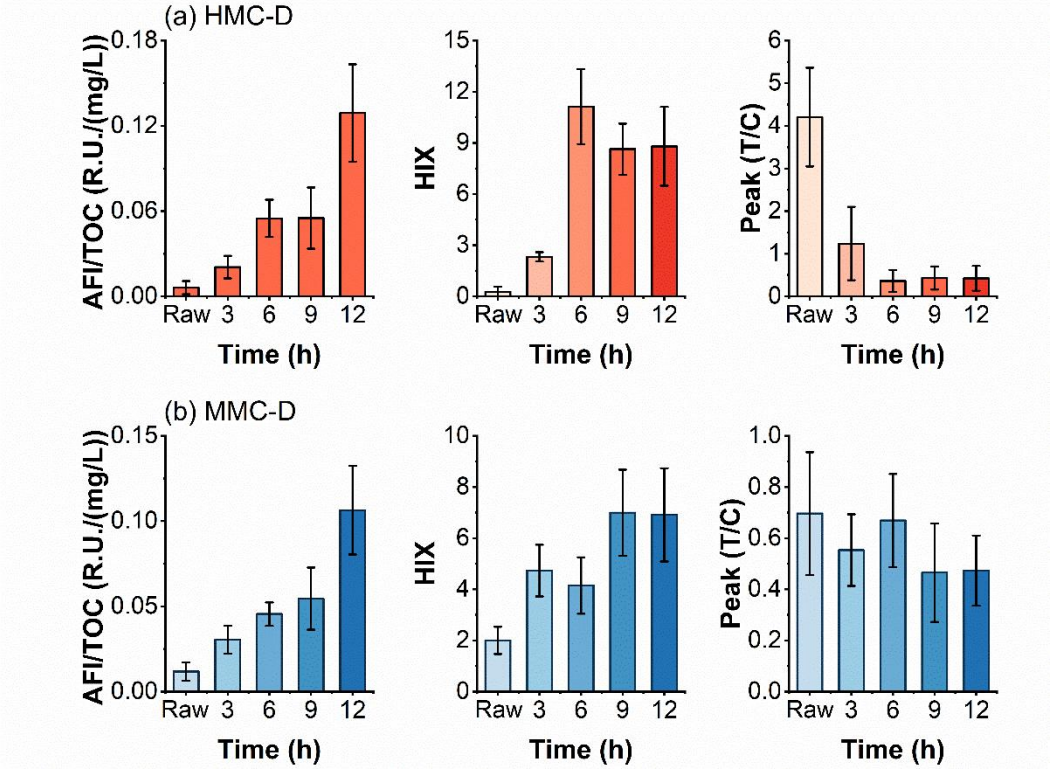

Figure 6. The variations in fluorescent indices of particle extracts during O_3 aging

The HIX and Peak (T/C) for HMC-D and MMC-D samples are presented in Figure 6. Higher HIX values are typically associated with a high degree of aromaticity and humification. The HIX of all samples increases with increasing aging time. After 12 hours of aging, the HIX for WSOC in HMC-D and MMC-D was 33.0 and 3.5 times of that of fresh samples, respectively. This indicates an enhancement in both the aromaticity and humification of WSOC during the aging process,

https://doi.org/10.5194/egusphere-2025-3084
Preprint. Discussion started: 1 September 2025

which further confirms the results in the above section regarding the elevation of both light absorption capacity and fluorescence intensity. Fan et al. (Fan et al., 2020) reported an increase in HIX of BrC from biomass burning by a factor of 2~3 after 24 h of O_3 aging. On the contrary, the Peak (T/C) generally decrease with the increase of aging time, dropping by 1.5 to 10 times after 12 h of aging, indicating that the aging of O_3 affects the biodegradation of organic matter.

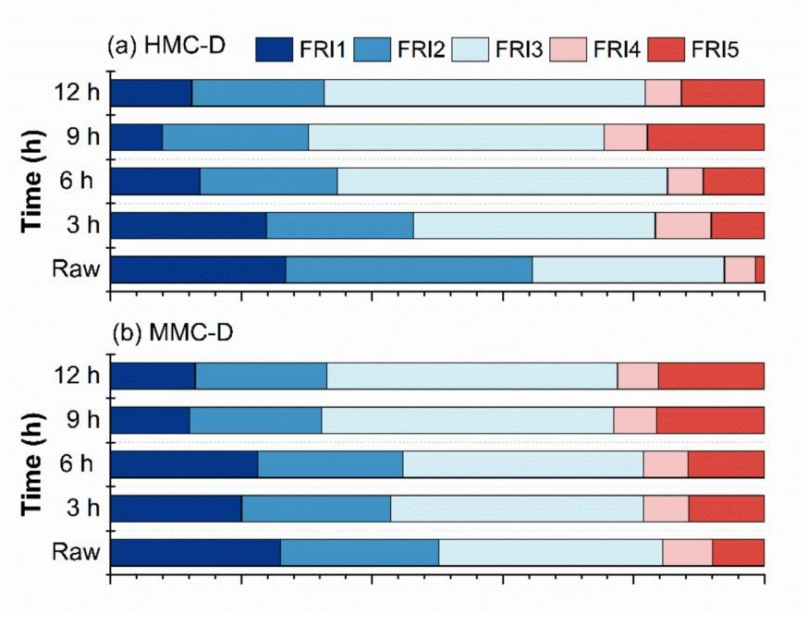

Figure 7. Distribution of fluorescence regional integration (FRI) during O_3 aging

3.3.4 FTIR analysis

The FTIR spectra of WSOC in HMC-D and MMC-D are illustrated in Figure 8. In the fresh WSOC of HMC-D samples, a variety of components containing hydroxyl, amine, carbonyl, and aromatic C=C groups aliphatic C-H can be identified (Huang et al., 2018; Popovicheva et al., 2019; Li et al., 2020; Zhang et al., 2020; Al-Abadleh, 2021; Hossen et al., 2023). FTIR spectra reveal changes in the chemical structure of WSOC in coal dust samples before and after O_3 aging. As anticipated, new N-H groups (peak position: 3296 cm^{-1}) appeared after 12 h of O_3 aging, likely contributing to the significant enhancement in the light absorption capacity of chromophores in HMC-D during the aging process (as indicated in Figure 5). Furthermore, we observe the formation of C-O groups at 1076 cm^{-1} in the HMC-D samples after 12 h of O_3 aging (Chen et al., 2016b). This change may be resulted from O_3 disrupting the aromatic ring and introducing oxygen-containing groups,

https://doi.org/10.5194/egusphere-2025-3084
Preprint. Discussion started: 1 September 2025

leading to the formation of aldehyde, ketone, and carboxylic acid compounds. The FTIR spectra of MMD-D are similar to those of HMC-D, which also show compositions containing hydroxyl, amine, carbonyl, and aromatic C=C groups. However, no new functional groups are observed in the MMD-D samples after aging. These observations suggest that while HMC-D experienced significant chemical changes during the aging process, MMD-D remained relatively stable in terms of its functional group composition. As a soluble component, WSOC has higher reactivity leading to more pronounced changes in its functional groups during aging compared to coal dust particles.

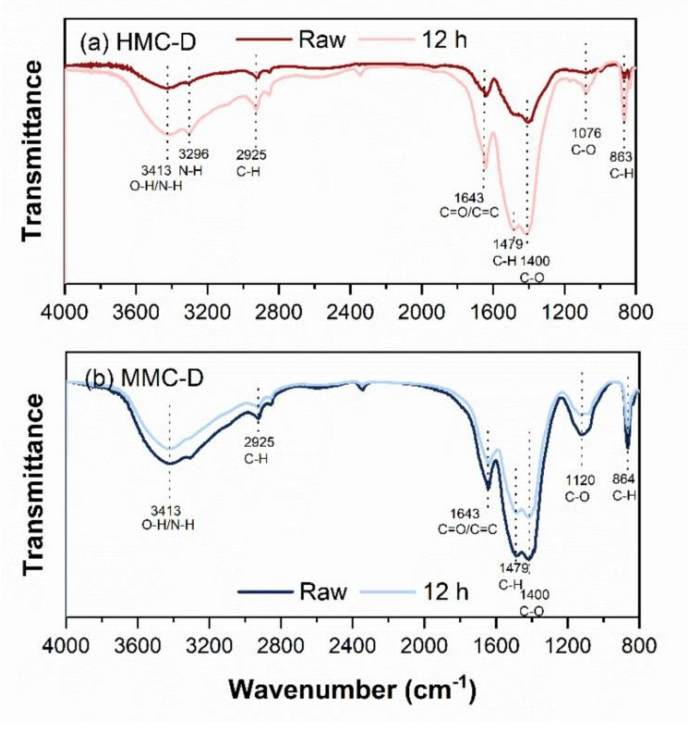

Figure 8. FTIR spectra of fresh and aging WSOC in (a) HMC-D and (b) MMC-D samples

4 Conclusions and implications

This study systematically investigates the effects of O_3 aging on the chemical and optical properties of WSOC in coal dust particles. FTIR and XPS analyses revealed that O_3 aging increases the oxygen content of coal dust particles and introduces new functional groups, such as COOH and C=O groups. These changes in chemical structure enhance the reactivity and hydrophilicity of WSOC. During O_3 aging, a variety of carbonyl compounds, particularly formaldehyde, acetaldehyde, and

https://doi.org/10.5194/egusphere-2025-3084
Preprint. Discussion started: 1 September 2025

acetone, were released from coal dust. In addition, the optical and chemical properties of WSOC changed significantly during O_3 aging, with a significant enhancement in the light-absorbing ability of WSOC and transformation of the protein-like fluorophores to humic-like fluorophores. In contrast, the light-absorbing ability in WSOC of MMC-D showed more pronounced changes that in HMC-D, attributable to the greater stability of aromatic structures in HMC-D.

The O_3 aging effect of coal dust has become more prevalent in the context of China's complex atmospheric particulate matter and O_3 pollution. The coal mining and washing industry emits about 1.93 million tons of particulate matter annually (Ministry of Ecology and Environment of China), and the substantial release of oxygenated volatile organic compounds during the aging process may exacerbate China's already complicated atmospheric pollution. Consequently, managers should rethink air quality improvement actions, especially in areas with intensive coal mining and transportation activities. Furthermore, O_3 aging significantly enhanced the MAE_{365} of WSOC by 8.8-18.2 times that of fresh samples, potentially affecting its role in the atmospheric radiative balance. To explore the potential effect of O_3 aging on WSOC radiative transfer, we have calculated the SFE, as shown in Figure 9. O_3-aged WSOC exhibited higher SFE values, with 12 h of aging (equivalent to 13 days of atmospheric aging) resulting in an underestimation of 0.2%-0.25% compared to fresh samples. These findings indicate that if atmospheric aging is not accounted for in making bulk aerosol measurements, the impact of WSOC absorption on SFE can be underestimated. Thus, we should re-examine how WSOC is handled in climate models, especially in areas with high coal dust emissions.

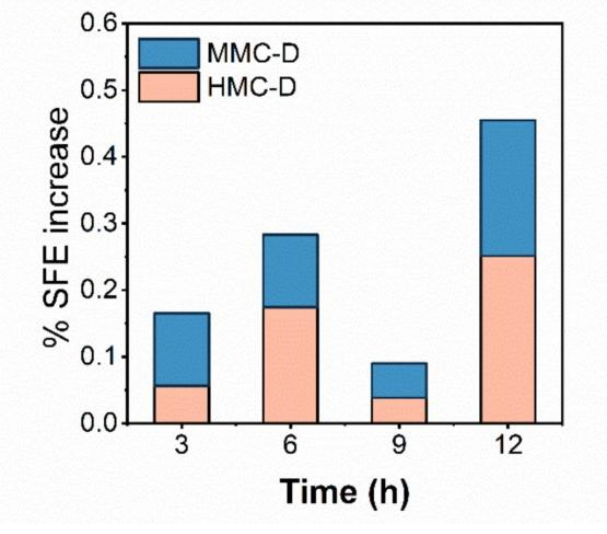

https://doi.org/10.5194/egusphere-2025-3084
Preprint. Discussion started: 1 September 2025

Figure 9. Percentage increase in the SFE of WSOC during O_3 aging relative to raw samples

Data availability. The data used in this study are available on the Zenodo data repository platform: https://doi.org/10.5281/zenodo.15767166 (Qin et al., 2025).

Author contribution. YQ: Writing – original draft, Visualization, Conceptualization. LY and JQ: Investigation. PY and JT: Writing – review & editing, Supervision, Funding acquisition. XZ: Investigation. CZ: Methodology. ZS: Validation. YG: Investigation. LZ: Methodology.

Competing interests. The authors declare that they have no conflict of interest.

Disclaimer. Publisher's note: Copernicus Publications remains neutral with regard to jurisdictional claims in published maps and institutional affiliations.

Financial support. This research was supported by the National Key Research and Development Program of China (grant no. 2022YFC3703400).

References

Abbasi, B., Wang, X., Chow, J. C., et al.: Review of respirable coal mine dust characterization for mass concentration, size distribution and chemical composition. Minerals, 2021, 11(4), 426.

Ahmad, S., Zeb, B., Ditta, A., et al.: Morphological, mineralogical, and biochemical characteristics of particulate matter in three size fractions (PM_{10}, $PM_{2.5}$, and PM_1) in the urban environment. ACS omega, 2023, 8(35), 31661–31674.

Al-Abadleh, H. A.: Aging of atmospheric aerosols and the role of iron in catalyzing brown carbon formation. Environmental Science: Atmospheres, 2021, 1(6), 297–345.

Azam, S., Liu, S., Bhattacharyya, S., et al.: Prevalence of nano-sized coal mine dust in North and Central Appalachian coal mines–Insights from SEM-EDS imaging. Journal of Hazardous Materials, 2024, 476, 135226.

Baduel, C., Monge, M. E., Voisin, D., et al.: Oxidation of Atmospheric Humic Like Substances by Ozone: A Kinetic and Structural Analysis Approach. Environmental Science and Technology, 2011, 45(12), 5238–5244.

Cardoso, A.: Behind the life cycle of coal: Socio-environmental liabilities of coal mining in Cesar, Colombia. Ecological Economics, 2015, 120, 71–82.

Chen, Q., Ikemori, F., and Mochida, M.: Light absorption and excitation–emission fluorescence of urban organic aerosol

https://doi.org/10.5194/egusphere-2025-3084
Preprint. Discussion started: 1 September 2025

components and their relationship to chemical structure. Environmental Science and Technology, 2016a, 50(20), 10859–10868.

Chen, Q., Ikemori, F., Higo, H., et al.: Chemical structural characteristics of HULIS and other fractionated organic matter in urban aerosols: results from mass spectral and FT-IR analysis. Environmental science and technology, 2016b, 50(4), 1721–1730.

Chen, Q., Li, J., Hua, X., et al.: Identification of species and sources of atmospheric chromophores by fluorescence excitation-emission matrix with parallel factor analysis. Science of the Total Environment, 2020, 718, 137322.

Chen, Y. and Bond, T.: Light absorption by organic carbon from wood combustion. Atmospheric Chemistry and Physics, 2010, 10(4), 1773-1787.

Coppola, A. I., Wagner, S., Lennartz, S. T., et al.: The black carbon cycle and its role in the Earth system. Nature Reviews Earth and Environment, 2022, 3(8), 516–532.

Dai, H., Yin, H., and Zhai, C.: Experimental investigation on the inhibition of coal dust deflagration by the composite inhibitor of floating bead and melamine cyanurate. Energy, 2022, 261, 125207.

Decesari, S., Facchini, M., Matta, E., et al.: Water soluble organic compounds formed by oxidation of soot. Atmospheric Environment, 2002, 36(11), 1827–1832.

EPA.U.S.: Determination of Formaldehyde in Ambient Air Using Adsorbent Cartridge Followed by High Performance Liquid Chromatography (HPLC), Compendium Method TO-11A in Compedium of Methods for the Determination of Toxic Organic Compounds in Ambient Air, 1999.

Ervens B, Kreidenweis S M. SOA formation by biogenic and carbonyl compounds: Data evaluation and application. Environmental science and technology, 2007, 41(11): 3904–3910.

Fan, X., Cao, T., Yu, X., et al.: The evolutionary behavior of chromophoric brown carbon during ozone aging of fine particles from biomass burning. Atmospheric Chemistry and Physics, 2020, 20(8), 4593–4605.

Guo, P. H.: Research and application of intermittent coal dust capture and recovery process Shandong University, 2021.

Horník, Š., Sýkora, J., Pokorná, P., et al.: Detailed NMR analysis of water-soluble organic compounds in size-resolved particulate matter seasonally collected at a suburban site in Prague. Atmospheric Environment, 2021, 267, 118757.

Hossen, M. A., Roy, S., Zaman, S. U., et al.: Emission of water soluble brown carbon from different combustion sources: optical properties and functional group characterisation. Environmental Research Communications, 2023, 5(8), 081002.

Huang, M., Xu, J., Cai, S., et al.: Characterization of brown carbon constituents of benzene secondary organic aerosol aged with ammonia. Journal of Atmospheric Chemistry, 2018, 75, 205–218.

Jane, S. F., Winslow, L. A., Remucal, C. K., et al.: Long - term trends and synchrony in dissolved organic matter characteristics in Wisconsin, USA, lakes: Quality, not quantity, is highly sensitive to climate. Journal of Geophysical Research: Biogeosciences, 2017, 122(3), 546–561.

Jiang, B., Zhou, Y., Ji, B., et al.: Investigation on the effect of functional groups on the wettability of coal dust: Experiments and theoretical validation. Fuel, 2023, 351, 128987.

Jiao, A., Tian, S., and Lin, H.: Analysis of outburst coal structure characteristics in Sanjia coal mine based on FTIR and XRD. Energies, 2022, 15(6), 1956.

Kamanzi, C., Becker, M., Jacobs, M., et al.: The impact of coal mine dust characteristics on pathways to respiratory harm:

https://doi.org/10.5194/egusphere-2025-3084
Preprint. Discussion started: 1 September 2025

investigating the pneumoconiotic potency of coals. Environmental Geochemistry and Health, 2023, 45(10), 7363–7388.

Kasap, Y. and Subaşı, E.: Risk assessment of occupational groups working in open pit mining: Analytic Hierarchy Process. Journal of Sustainable Mining, 2017, 16(2), 38–46.

Khan, A. L., Dierssen, H., Schwarz, J. P., et al.: Impacts of coal dust from an active mine on the spectral reflectance of Arctic surface snow in Svalbard, Norway. Journal of Geophysical Research: Atmospheres, 2017, 122(3), 1767–1778.

Kuang, Y. and Shang, J.: Changes in light absorption by brown carbon in soot particles due to heterogeneous ozone aging in a smog chamber. Environmental Pollution, 2020, 266, 115273.

Kuang, Y., Shang, J., and Chen, Q.: Effect of ozone aging on light absorption and fluorescence of brown carbon in soot particles: The important role of polycyclic aromatic hydrocarbons. Journal of Hazardous Materials, 2021, 413, 125406.

Li, C., He, Q., Fang, Z., et al.: Laboratory insights into the diel cycle of optical and chemical transformations of biomass burning brown carbon aerosols. Environmental science and technology, 2020, 54(19), 11827–11837.

Li, Q., Shang, J., Liu, J., et al.: Physicochemical characteristics, oxidative capacities and cytotoxicities of sulfate-coated, 1,4-NQ-coated and ozone-aged black carbon particles. Atmospheric Research, 2015, 153, 535–542.

Liu, X., Li, L., and Yang, Y.: Development status of coal mining in China. Journal of the Southern African Institute of Mining and Metallurgy, 2023, 123(1), 19–28.

Mischler, S. E., Cauda, E. G., Di Giuseppe, M., et al.: Differential activation of RAW 264.7 macrophages by size-segregated crystalline silica. Journal of Occupational Medicine and Toxicology, 2016, 11, 1–14.

Popovicheva, O. B., Engling, G., Ku, I. T., et al.: Aerosol emissions from long-lasting smoldering of boreal peatlands: chemical composition, markers, and microstructure. Aerosol and Air Quality Research, 2019, 19(3), 484–503.

Qin, Y., Yi L., Yi P., et al.: Measurement report: Evolution of water-soluble organic carbon in neglected coal dust particles influenced by ozone aging [Data set]. Zenodo. https://doi.org/10.5281/zenodo.15767166, 2025.

Sareen, N., Moussa, S. G., and McNeill, V. F.: Photochemical aging of light-absorbing secondary organic aerosol material. The Journal of Physical Chemistry A, 2013, 117(14), 2987–2996.

Snyder, D. C., Rutter, A. P., Collins, R., et al.: Insights into the origin of water soluble organic carbon in atmospheric fine particulate matter. Aerosol Science and Technology, 2009, 43(11), 1099–1107.

Sun, Y., Zhang, Q., Zheng, M., et al.: Characterization and source apportionment of water-soluble organic matter in atmospheric fine particles ($PM_{2.5}$) with high-resolution aerosol mass spectrometry and GC–MS. Environmental science and technology, 2011, 45(11), 4854–4861.

Vanka, K. S., Shukla, S., Gomez, H. M., et al.: Understanding the pathogenesis of occupational coal and silica dust-associated lung disease. European Respiratory Review, 2022, 31(165), 210250.

Xiang, P., Zhou, X., Duan, J., et al.: Chemical characteristics of water-soluble organic compounds (WSOC) in $PM_{2.5}$ in Beijing, China: 2011–2012. Atmospheric Research, 2017, 183, 104–112.

Xiao, K., Shen, Y., Sun, J., et al.: Correlating fluorescence spectral properties with DOM molecular weight and size distribution in wastewater treatment systems. Environmental Science: Water Research and Technology, 2018, 4(12), 1933–1943.

Xu, C., Wang, D., Wang, H., et al.: Effects of chemical properties of coal dust on its wettability. Powder Technology, 2017, 318, 33–39.

https://doi.org/10.5194/egusphere-2025-3084
Preprint. Discussion started: 1 September 2025

Yan, J., Lei, Z., Li, Z., et al.: Molecular structure characterization of low-medium rank coals via XRD, solid state ^{13}C NMR and FTIR spectroscopy. Fuel, 2020, 268, 117038.

Yang, Y., Qin, J., Qi, T., et al.: Fluorescence characteristics of particulate water-soluble organic compounds emitted from coal-fired boilers. Atmospheric Environment, 2020, 223, 117297.

Zhang, H., Shen, L., Zhong, S., et al.: Economic structure transformation and low-carbon development in energy-rich cities: The case of the contiguous area of shanxi and shaanxi provinces, and inner Mongolia Autonomous Region of China. Sustainability, 2020, 12(5), 1875.

Zhao, Q., Liu, J., Huang, C., et al.: Characteristics of coal dust deflagration under the atmosphere of methane and their inhibition by coal ash. Fuel, 2021, 291, 120121.

Zhou, X. M., Zhuang, X. G., and Shangguan, Y. F., et al: Mineralogical and geochemical characteristics of the dust of vent from the underground coal mines in Ningwu Coalfield, Shanxi Province, submitted. 2024.

Zhou, Y., Liu, J., Jin, L., et al.: Physicochemical characteristics and their variation of coal dust originating from underground mining sites. ACS Omega, 2025, 10(6), 5379–5394.